ACS APPLIED MATERIALS & INTERFACES

Research Article

Cite This: ACS Appl. Mater. Interfaces 2019, 11, 48512−48517

www.acsami.org

Highly Floatable Superhydrophobic Metallic Assembly for Aquatic Applications

Zhibing Zhan,[†] Mohamed ElKabbash,[†] JinLuo Cheng,[‡] Jihua Zhang,[†] Subhash Singh,[†] and Chunlei Guo*[,†]

[†]The Institute of Optics, University of Rochester, Rochester, New York 14627, United States

[‡]Changchun Institute of Optics, Fine Mechanics, and Physics, Changchun 130033, China

Supporting Information

ABSTRACT: Water-repellent superhydrophobic (SH) surfaces promise a wide range of applications, from increased buoyancy to drag reduction, but their practical use is limited. This comes from the fact that an SH surface will start to lose its efficiency once it is forced into water or damaged by mechanical abrasion. Here, we circumvent these two most challenging obstacles and demonstrate a highly floatable multifaced SH metallic assembly inspired by the diving bell spiders and fire ant assemblies. We study and optimize, both theoretically and experimentally, the floating properties of the design. The assembly shows an unprecedented floating ability; it can float back to the surface even after being forced to submerge under water for months. More strikingly, the assembly maintains its floating ability even after severe damage and piercing in stark contrast to conventional watercrafts and aquatic devices. The potential use of the SH floating metallic assembly ranges from floating devices and electronic equipment protection to highly floatable ships and vessels.

KEYWORDS: *superhydrophobic surface, trapped air, femtosecond laser ablation, highly floatable assembly, aquatic application*

INTRODUCTION

Water-repellent superhydrophobic (SH) surfaces promise a wide range of applications, from increased buoyancy to drag reduction,[1−6] but their practical use is limited.[3] Typically, SH surfaces require extensive nano- and microscale surface textures, and in most cases, superhydrophobicity comes from a layer of air trapped among these structures.[5,7−10] This underlying mechanism imposes two fundamental hurdles that prevent SH surfaces from widespread use. First, once they are entirely submerged into water, SH surfaces will wet over time and relent their SH response.[11−13] Second, the surface texture is susceptible to mechanical wear and abrasion, which can quickly degrade and eventually extinguish the surface superhydrophobicity.[1,3,14,15] Here, we circumvent both these obstacles and demonstrate a highly floatable multifaced SH metallic assembly inspired by the diving bell spiders (*Argyroneta aquatica*) and fire ant assemblies that trap a large amount of air with their SH body surfaces even fully submerged under water without releasing the air cushion.[5] We study, both theoretically and experimentally, the floating properties of the design. The assembly maintains its floating ability even after severe damage and piercing. We envision the applications of our highly floatable SH assemblies to range from replacing personal floating devices to electronic equipment protection and, eventually, large aquatic vessels to create super-floatable boats or ships. Other materials can be processed to become SH, and future research directions can include flexible materials to create floating, high loading capacity wearable devices and clothes that maintain their floating properties even after tearing or piercing.

RESULTS AND DISCUSSION

A. aquatica spiders live their entire lives underwater while maintaining a terrestrial respiratory system; that is, they breathe air.[16] The spiders create a dome-shaped web, so-called diving bell, between aquatic plants underwater and fill the diving bell with air carried from the water surface by trapping air between their SH legs and abdomen and within the SH diving bell. The ability of these creatures to sustain the SH functionality indicates that they evolved to maintain their superhydrophobicity even after being fully submerged in water indefinitely. Furthermore, fire ants can self-assemble and form a raft by trapping a large volume of air among their SH bodies.[17] The key insight is that multifaced SH surfaces can trap a large air volume, which points toward the possibility of using SH surfaces to create buoyant devices for aquatic applications. Inspired by these two species, we present a design of a highly floatable device. We note that a single SH metal can

Received: August 28, 2019
Accepted: November 6, 2019
Published: November 6, 2019

DOI: 10.1021/acsami.9b15540
ACS Appl. Mater. Interfaces 2019, 11, 48512−48517

float on the water surface;[4,18,19] however, if a force is exerted downward, exceeding the loading capacity, then the SH metal will permanently sink and relent its SH properties; that is, even after it is brought back to the surface, it may not float (Figure 1a and Movie S1 in the Supporting Information). Our assembly consists of two parallel aluminum (Al) plates that are treated to become SH and connected by a plastic post (Figure 1b and Figure S1). The two SH surfaces face each other so that they are enclosed and free from external wear and abrasion, while the outer surfaces are regular untreated Al. Because of the water repellency of the SH surfaces, this assembly will trap a large volume of air under water and the assembly will float back to the surface even after being forced into water (Figure 1e and Movie S1). Figure 1d shows that an SH assembly forced to submerge under water by a load traps an air bubble between the metal plates (Figure 1d, inset). After the load is released, the SH assembly floats back to the surface (Figure 1e and Movie S2). On the other hand, the same assembly consisting of two untreated Al disks remains sunk, and no air is trapped between the disks (see Figure 1d, Figure S1, and Movie S3).

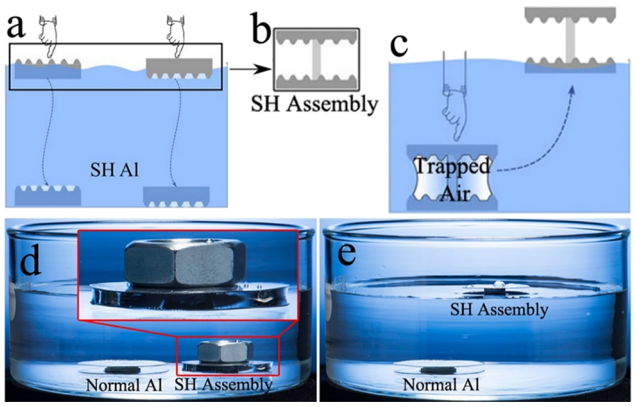

Figure 1. Design principle of the highly floatable superhydrophobic metallic assembly. (a–c) Schematics show that two SH Al disks (a) sink to the bottom of the beaker after piercing the water surface. (b) Design of the SH assembly consisting of two Al disks such that their inner surfaces are treated to be SH. The Al disks are connected by a plastic post. (c) An SH assembly forced to sink under water will float back to the surface when the load is released. (d) Image of the assembly forced to sink due to a heavy load while trapping an air bubble between the SH Al disks. The same assembly with bare Al, however, is unable to float. (e) Image showing the SH assembly floating back to the surface after the load is released.

A surface is considered SH if a water droplet beads up on the surface with a contact angle (CA) $\theta > 150°$.[2,20−23] To create an SH Al surface, we use a direct femtosecond (fs) laser processing technique to produce a range of hierarchical micro- and nanostructures on Al. An fs laser technique can directly create micro/nanoscale hierarchical structures on a wide variety of materials by a simple one-step scanning method,[7,24] which is a powerful method for research of various special surface wetting properties.[7,15,20,22,24−32] To further control the degree of hydrophobicity, we control the surface morphology by varying the laser processing conditions and the surface energy by immersing the structured Al surface in aqueous ethanol solution of stearic acid for various durations. Details on the experimental setup and fabrication processes are described in the Supporting Information (Methods section). Without fs laser treatment, CA for bare Al is only ~54° (see Figure 2a,b). Similar to our previous works,[7,24] fs laser processing also turns the treated area pitch black with the near-unity optical absorption (Figure 2c).[7,24] As shown in Figure 2d, Al becomes black and SH with $\theta \approx 168°$ following fs laser and chemical treatments. Figure 2e,f shows scanning electron microscopy (SEM) images of typical hierarchical micro- and nanostructures that formed on the Al surface following fs laser treatment. The structure consists of an array of microgrooves (Figure 2e) covered by extensive nanostructures (Figure 2f; also see Figure S2 for more SEM images). The surface morphology is also measured using a confocal UV

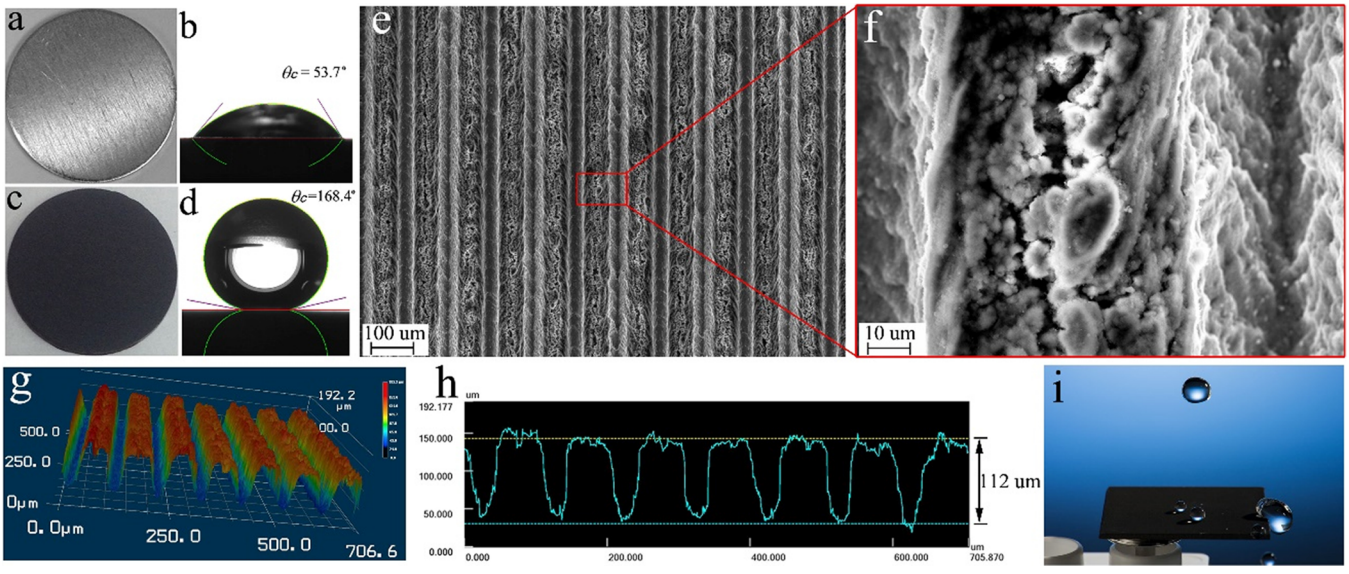

Figure 2. Femtosecond laser-treated SH Al surface. (a–d) Sample photos and corresponding water CA of a bare Al surface (a, b) and that with fs laser treatment and stearic acid modification (c, d). (e, f) SEM images of Al surfaces after fs laser treatment. (g, h) Confocal UV laser microscopy image of the three-dimensional surface profile (g) and a cross section showing the height variation (h). (i) Photo of water droplets bouncing off the fs laser-treated SH surface.

DOI: 10.1021/acsami.9b15540
ACS Appl. Mater. Interfaces 2019, 11, 48512−48517

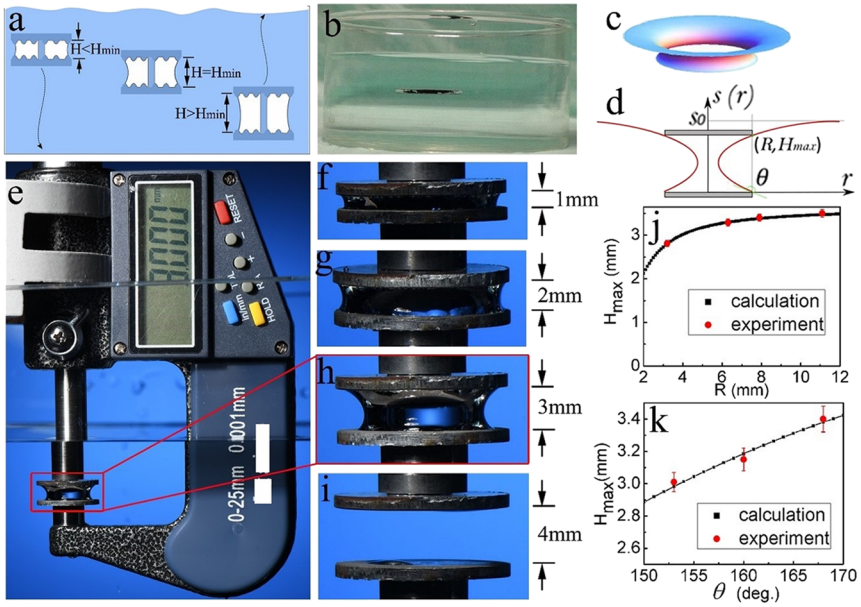

Figure 3. Design parameters: determination of the gap distance range of multifaced SH assembly. (a) Schematic of the gap distance (H) effect on the assembly buoyancy. (b) Image of the assembly with $H = H_{min}$ staying stationary in water. (c, d) Calculated topography of the dimple formed on the water surface after placing a single SH surface (c) and schematic illustrating the dependence of H_{max} on R and θ (d). (e) Photo of the experimental setup used to determine H_{max}. (f–i) Photos of the trapped air underwater with H = 1.0 mm (f), H = 2.0 mm (g), H = 3.0 mm (h), and H = 4.0 mm (i). (j, k) Experimental and calculated results of the largest gap distance (H_{max}) as a function of the SH surface radius (j) and CA (k).

laser microscope, as shown in Figure 2g,h. The strong water repellency of our SH Al is captured by a water droplet bouncing from the surface shown in Figure 2i and Movie S4.

The gap distance between the two Al plates, H, is a key parameter in our design. There is a minimum H value for the assembly to trap enough air to keep itself afloat (H_{min}) (see Figure 3a). A larger H will trap more air and increase the buoyancy and loading capacity of the device; however, there exists a maximum H where the assembly loses its buoyancy as it can no longer trap air inside (H_{max}). Therefore, our first study is to determine the admissible range of H for the assembly to stay afloat. H_{min} is determined by equating the weight of the overall assembly to the displaced water. Using our assembly with the Al disk thickness of 0.2 mm, H_{min} is ~0.68 mm (see the Supporting Information). This value agrees with our experimentally observed value of 0.761 mm (Figure S3), where the assembly will remain stationary, neither rise nor sink (Figure 3b). The discrepancy between calculated and demonstrated H_{min} is due to the approximation in the calculations and the additional weight of the plastic post and glue used for preparing the assembly (Figure S1). Note that H_{min} is independent of the Al disk radius (R).

Next, we investigate the maximum possible gap distance, H_{max}, as a function of the Al disk radius and surface hydrophobicity. To find H_{max} theoretically, our approach is to consider a single SH plate with radius R floating on the water surface. The water surface will form a dimple, and the dimple topography $s(x, y)$, at equilibrium, is determined by the Young–Laplace equation, $\rho_W g s = \sigma \nabla \cdot \hat{n}$, where ρ_W is the water density, σ is the water–air interfacial energy, g is the gravity constant, $s = s(x, y)$ is the formed dimple surface, and $\hat{n} = \hat{n}(x, y)$ is the surface normal vector.[19,33−35] In our system, the Young–Laplace equation can be expressed in a polar coordinate as follows

$$\frac{\rho_W g}{\sigma}(s - s_0) = \frac{1}{r}\frac{\mathrm{d}}{\mathrm{d}r}\frac{rs'(r)}{\sqrt{1 + [s'(r)]^2}} \quad (1)$$

where $s_0 = s(\infty)$ is the dimple height from the water surface at infinity, that is, approaching the waterline where the dimple vanishes. By setting $\xi = \rho_W g/\sigma$ and $s'(r) = \tan \varphi$ with $\varphi \in (0, \theta]$ (θ is the CA), the above equation can be converted to the parameter space as

$$\frac{\mathrm{d}r(\varphi)}{\mathrm{d}\varphi} = \frac{r(\varphi)\cos \varphi}{\xi r(\varphi)[s_0 - s(\varphi)] + \sin \varphi} \quad (2)$$

$$\frac{\mathrm{d}s(\varphi)}{\mathrm{d}\varphi} = \tan \varphi \frac{\mathrm{d}r(\varphi)}{\mathrm{d}\varphi} \quad (3)$$

$$r(\theta_c) = R,\ s(\theta_c) = 0 \quad (4)$$

For a given s_0, the above differential equations can be solved numerically. The real solution is obtained when the given s_0 satisfies $s_0 = s(\varphi = 0)$. When the top Al plate has the same radius as the bottom plate, the maximum gap distance that enables air trapping is $H_{max} = s(\varphi_0)$ on the surface, with φ_0 being different from θ and satisfying $r(\varphi_0) = R$. The calculated 3D dimple topology is shown in Figure 3c, and the dependence of H_{max} on the diameters and on the CAs of the SH Al surfaces is shown in Figure 3j,k (all data can be found in Table S1, Supporting Information). The calculation details are presented in the Supporting Information.

To determine H_{max} experimentally, we use a high-resolution digital micrometer and attach two aligned Al SH surfaces to the micrometer legs. First, we have the two surfaces touching each other and reset the digital micrometer to zero (see Figure S4). Next, we increase the gap distance outside of water, set it to a certain value, and adiabatically immerse the assembly to ~1 cm (see Figure 3e) below the water surface. The adiabatic process here means that the SH assembly is immersed into the water rapid enough that the trapped air does not leak out. The

DOI: 10.1021/acsami.9b15540
ACS Appl. Mater. Interfaces 2019, 11, 48512−48517

beaker is filled with water to ~5 cm high, and the water pressure variation over the 5 cm height of water is ~0.5% of atmospheric pressure so that the effect of the water depth is negligible. Since our study focuses on the floating effect and the SH assembly always floats back to the surface after being forced into water, we neglect the deep-water pressure effect and leave it for future investigations. For small H, 1 mm here, the trapped air bubble takes an approximate shape of a cylinder close to the diameter of the disk (Figure 3f). When H increases to 2 and 3 mm, the trapped air takes a clearer form of a hyperboloid (Figure 3g,h). Finally, at H = 4 mm, the SH plates are incapable of trapping air (Figure 3i). To study the dependence of H_{max} on the disk radius R and the water−solid CA, we fabricate a series of samples with R = 3.2, 6.3, 7.9, and 11.1 mm with θ = 168° (Figure S5) and CA $\theta \approx$ 153°, 160°, and 168° with R = 7.9 mm (Figure S6). Figure 3j shows the experimental and calculated results for H_{max} as a function of R (two examples are shown in Figure S7). For smaller R values, H_{max} increases with R, while for larger R values, H_{max} becomes constant. Figure 3k shows the experimental and calculated results for H_{max} as a function of CA. As expected, a larger CA (stronger hydrophobicity) results in a larger H_{max}.

Experimentally, as we submerge the assembly adiabatically into the water, there will be air loss during the submersion process and this air loss is more pronounced with a larger initial gap distance. Therefore, the diameter of the trapped air column decreases with gap distance H, as shown in Figure 3. Accordingly, it is difficult to quantitatively estimate the volume of the trapped air only by knowing H. For example, it is difficult to tell if the volume of the entrapped air in Figure 3h is greater than that in Figure 3g, although Figure 3h has a larger H. To determine the H value that gives the maximum buoyancy force F_b, we started with an initial gap distance H_1 and then reduced the gap distance underwater to minimize the curvature so that the trapped air takes the form of an ideal cylinder that has a radius R and a gap distance H_2 (see schematic in Figure 4a). Example images of the trapped air column with H_1 = 2.75 mm and H_2 = 2.338 mm are shown in Figure 4b,c, respectively, for an assembly of R = 11.1 mm and θ = 168° (see Figure S8). For a given H_1, the trapped air volume and the corresponding buoyancy force F_b can be readily calculated using H_2 according to the following equation: $F_b = \rho_W g\pi R^2(H_2 + 2h_M)$, where R and h_M are the radius and thickness of our Al SH plates (11.1 and 0.2 mm in this case), respectively. The calculated results for F_b are shown in Figure 4d (black circles). The linear change of H versus H_1 is also plotted in Figure 4d. For SH Al disks of R = 11.1 mm, when H_1 < 2.75 mm, H_2 increases with H_1, which means that, by simply increasing the gap distance, the trapped air volume, and buoyancy, increases. For H_1 > 2.75 mm, H_2 decreases with H_1 due to the decrease in the trapped air radius that we noted earlier when comparing Figure 3g,h. In the demonstrated case, the largest buoyancy force for the SH Al assembly corresponds to $H_1 \approx$ 2.75 mm. Therefore, we prepared an assembly with H = 2.75 mm and R = 11.1 mm and tested its loading capacity. The assembly can float back to the water surface even with a load of 2.5 times its weight (Movie S5 and Figure S9). The maximum loading capacity (1.021 g here) agrees well with the calculated maximum buoyancy shown in Figure 4d (F_b = 0.01043 N, which corresponds to 1.064 g). If the intended application is to create a floating device with high loading capacity, then we note that it is sufficient to only transform the outer rim of the metal plates to be SH instead of the entire

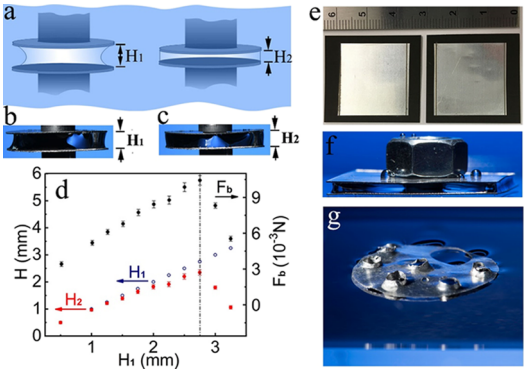

Figure 4. Applications: loading capacity and durability after severe damage. (a) Schematic of the gap distances H_1 and H_2: we started with an initial gap distance H_1 and then reduced the gap distance underwater to minimize the gap so that the trapped air will take the form of an ideal cylinder that has radius R and gap distance H_2. (b, c) Photos of the trapped air topology in water for an initial gap distance (H_1) (here, 2.75 mm) (b) and the gap distance where the trapped air takes the form of a regular cylinder in water (H_2) (here, 2.338 mm) (c). (d) Dependence of H_2 on H_1 and the corresponding buoyancy force (F_b) based on H_2. (e) Two Al squares with an area of ~30 mm × 30 mm with only ~3 mm width frame treated with an fs laser to be SH (black frame). (f) SH assembly based on the Al squares shown in (e) submerged under water with a heavy load while trapping an air bubble. (g) An SH assembly remains floating even after significant structural damage (six smaller through holes each with a 3 mm diameter and one larger through hole with a 6 mm diameter).

plates, as shown in Figure 4e. Indeed, the device will trap an air bubble and remain afloat after releasing a load, as shown in Figure 4f and Movie S6. For an assembly with a given H, the loading capacity scales with R^2; for example, for H = 2.75 mm, an assembly with R = 13.82 m can handle a load of 1 ton, while the required area treated to be SH is only ~0.5 m^2 (see Figures S10 and S11).

Although the SH surface textures are susceptible to mechanical wear and tear, our design overcomes this problem since the SH surfaces are enclosed within the assembly and they are in direct contact with neither any external load nor the water. For the durability test, a loaded SH assembly has been left in water for 2 months, and the assembly remains floating for the entire period without sinking or any observed deterioration. We note that the trapped air remains under water due to loading for the entire period (see Figure S9). Another important advantage of the SH assembly is that, although the floating principle is the same as other floating devices, for example, ships, the assembly structure can withstand severe damage and even substantial piercing without sinking. If the air entrapment was due to conventional methods of concealment, then water will rush inside the device after piercing, for example, damaging a ship's hull or piercing a personal floating device, and it will sink if the floating object is denser than water. However, in our design, the SH assembly automatically conceals the entrapped air even if the SH metals are pierced, and water replaces the trapped air within the pierced volume (Figure 4g). In principle, no matter how many holes are drilled through the assembly, the structure will float because the water volume is replaced by water so the buoyancy condition of the entire structure is still satisfied (schematics shown in Figure S12). Figure 4g shows a severely pierced SH assembly (~20% of the structure is removed) without affecting its ability to float (see Movie S7). Clearer images show the

DOI: 10.1021/acsami.9b15540
ACS Appl. Mater. Interfaces 2019, 11, 48512−48517

severely pierced SH assembly on water surface, as shown in Figure S13. No water rushes inside the assembly, which is in stark contrast to conventional buoyant devices composed of denser-than-water materials. Furthermore, the severely pierced SH assembly can float back to the water surface very quickly (~2.5 s) even after being immersed in a deep (44 cm) container, as shown in Movie S8. Note, a watercraft or a personal floating device made of denser-than-water material(s) would sink if pierced. On the other hand, the existence of two SH plates conceals the trapped air automatically after piercing, and no water can rush inside the plates, which is a unique property for our assembly.

CONCLUSIONS

This work demonstrated how to use SH effects to render metals highly floatable. Our design overcame the most fundamental hurdles preventing SH surfaces from practical applications, namely, wetting the SH surface after being submerged into water and mechanical wear and tear. The work serves as a starting point to develop biomimetic designs inspired by creatures utilizing their SH surfaces even if they are fully submerged under water. The ability of the SH assemblies to remain afloat after severe structural damage is unique compared to conventional floating devices and watercrafts that have been used for millennia. Using a stack of SH assembly can further increase the loading capacity per unit surface area, which is more suitable for constructing large aquatic vessels. The applications of the highly floatable SH assembly can range from constructing personal floating devices and electronic equipment protection to floatable boats or ships. For example, inflatable floating devices cannot float after piercing, which can be overcome using our design concept. As other materials can be processed to become SH, future research can investigate flexible materials to create floating and high loading capacity wearable devices that can survive tearing and piercing.

EXPERIMENTAL SECTION

Aluminum plates with thickness values of 0.2 and 1.0 mm with purity of 99.9% were purchased from Goodfellow and degreased in acetone before laser ablation. Stearic acid (98%) and absolute ethanol were purchased from Alfa Aesar. All chemicals were analytical grade reagents and were used as received.

The Al was first processed by femtosecond (fs) laser pulses to obtain hierarchical micro- and nanoscale surface structures, as shown in Figure S14. In our experiments, an amplified Ti:sapphire laser system was used that generates 65 fs pulses with a central wavelength of 800 nm and at a maximum pulse repetition rate of 1 kHz. The laser beam was focused onto the sample surface mounted on a computerized XY-translation stage. The pulse energy from the fs laser was ~0.8 mJ, and the linear velocity of the translation stage is 1 mm/s. To control the superhydrophobicity, we also use pulse energies of 0.4 and 0.2 mJ. The period between the adjacent scanning lines is 100 μm. To further control the degree of hydrophobicity, we control the surface morphology by varying the laser processing conditions and the surface energy by immersing the structured Al surface in aqueous ethanol solution of stearic acid (0.01 M) for various durations. Afterward, the sample was rinsed by pure ethanol and dried in a 60 °C oven for 30 min.

A water droplet with a diameter of ~2.8 mm was generated from a syringe tip that was connected to a syringe pump. Water droplets were dropped from a height of 80 mm (tip to surface). The spreading and retraction dynamics of the droplet on the surfaces were recorded using a high-speed camera (NAC, HotShot 1280 cc) with 3000 frames/s.

SH assemblies were prepared by using plastic rings with different heights to control the gap distances between two SH Al plates, as shown in Figure S1. The plastic rings were first cut from a plastic tube with an outside diameter of ~7.0 mm and a tube thickness of 0.9 mm. The rings were then abraded by sandpapers to obtain the desired height to control the gap distance in the SH assembly. An epoxy (Loctite EA 450 A&B) was used to glue the plastic post to the two aligned SH Al plates to form an Al SH assembly. The two SH Al surfaces face each other so that they are enclosed and free from external wear and abrasion, while the outer surfaces can be regular untreated Al. Finally, the SH assembly was placed in an oven with a temperature of 50 °C for 60 min to dry totally. The additional load test was carried out by sticking an Al plate with the radius of 11.1 mm and thickness of 1.0 mm on the bottom of the assembly to avoid the overturning of the sample when it is floating to the water surface. To test the piercing effect, the SH assembly was purposely damaged by drilling several holes on the SH assembly.

The surface structures were first analyzed by a confocal UV scanning laser microscope (KEYENCE, VK-9700) that resolves microstructures and provides a larger viewing area. For a more detailed view, a scanning electron microscope was used to determine micro- and nanoscale surfaces down to 10 nm resolution. It is a Zeiss Auriga field emission scanning electron microscope operating at an accelerating voltage of 20 kV. The surface CA values were measured by a Kino SL200KB contact angle meter.

ASSOCIATED CONTENT

Supporting Information

The Supporting Information is available free of charge at https://pubs.acs.org/doi/10.1021/acsami.9b15540.

Photos of normal and SH assemblies, SEM images of the SH Al surface, photos of the SH assembly with H_{min} and the digital micrometer used in this work, SH surfaces with different diameters, SEM images and photos of SH surfaces with different contact angles, photos of the samples to determine H_{max} and F_b, loading test of the SH assembly, schematics of the loading capacity and treated areas of the SH assembly, schematics of the air volume of a severely pierced SH assembly and its photos, experimental setup for fs laser processing, detailed calculation processes of H_{min} and H_{max}, and descriptions of additional movies showing the SH Al surface, SH assembly, and floating properties of the assemblies (PDF)

Single SH Al disk sinking after a force is exerted downward, exceeding the loading capacity, and SH assembly floating back to the surface even after being forced into water (MOV)

SH assembly floating back to the water surface once the load is released and normal Al disks remaining sunk (MOV)

Comparison of a regular Al assembly and an SH assembly (MP4)

Water bouncing dynamics from an SH Al surface (MP4)

Optimized SH assembly floating on the water surface with a maximum loading of 1.021 g (MP4)

Square-shaped SH assembly with only the outermost rim turned to be SH showing the same floating behavior as a fully treated assembly (MP4)

Severely damaged SH assembly also floating back to the water surface after being forced into water (MOV)

Severely damaged SH assembly floating back to the water surface very fast (~2.5 s) after being forced into water as deep as 44 cm (MP4)

DOI: 10.1021/acsami.9b15540
ACS Appl. Mater. Interfaces 2019, 11, 48512−48517

AUTHOR INFORMATION

Corresponding Author

*E-mail: guo@optics.rochester.edu.

ORCID

Chunlei Guo: 0000-0001-8525-6301

Notes

The authors declare no competing financial interest.

ACKNOWLEDGMENTS

This work was supported by the Bill & Melinda Gates Foundation (OPP1157723), the US Army Research Office (W911NF-15-1-0319), and National Science Foundation (1701163 and 1722169) grants. The authors would like to acknowledge A. Fenster and M. Mann for their assistance in recording high-quality photos and videos and J.-H. Kim and J. Shang for their assistance in recording water bouncing videos.

REFERENCES

(1) Lu, Y.; Sathasivam, S.; Song, J.; Crick, C. R.; Carmalt, C. J.; Parkin, I. P. Robust Self-Cleaning Surfaces that Function when Exposed to either Air or Oil. *Science* **2015**, *347*, 1132−1135.

(2) Liu, T.; Kim, C.-J. Turning a Surface Superrepellent Even to Completely Wetting Liquids. *Science* **2014**, *346*, 1096−1100.

(3) Tian, X.; Verho, T.; Ras, R. H. A. Moving Superhydrophobic Surfaces Toward Real-World Applications. *Science* **2016**, *352*, 142−143.

(4) Pan, Q.; Wang, M. Miniature Boats with Striking Loading Capacity Fabricated from Superhydrophobic Copper Meshes. *ACS Appl. Mater. Interfaces* **2009**, *1*, 420−423.

(5) Tiginyanu, I.; Braniste, T.; Smazna, D.; Deng, M.; Schütt, F.; Schuchardt, A.; Stevens-Kalceff, M. A.; Raevschi, S.; Schürmann, U.; Kienle, L.; Pugno, N. M.; Mishra, Y. K.; Adelung, R. Self-Organized and Self-Propelled Aero-GaN with Dual Hydrophilic-Hydrophobic Behaviour. *Nano Energy* **2019**, *56*, 759−769.

(6) Nyström, G.; Fernández-Ronco, M. P.; Bolisetty, S.; Mazzotti, M.; Mezzenga, R. Amyloid Templated Gold Aerogels. *Adv. Mater.* **2016**, *28*, 472−478.

(7) Vorobyev, A. Y.; Guo, C. Multifunctional Surfaces produced by femtosecond laser pulses. *J. Appl. Phys.* **2015**, *117*, 033103.

(8) Gao, X.; Jiang, L. Water-Repellent Legs of Water Striders. *Nature* **2004**, *432*, 36−36.

(9) Peaudecerf, F. J.; Landel, J. R.; Goldstein, R. E.; Luzzatto-Fegiz, P. Traces of Surfactants Can Severely Limit the Drag Reduction of Superhydrophobic Surfaces. *Proc. Natl. Acad. Sci. U. S. A.* **2017**, *114*, 7254−7259.

(10) Zhan, Z.; Li, Z.; Yu, Z.; Singh, S.; Guo, C. Superhydrophobic Al Surfaces with Properties of Anticorrosion and Reparability. *ACS Omega* **2018**, *3*, 17425−17429.

(11) Lee, C.; Kim, C.-J. Underwater Restoration and Retention of Gases on Superhydrophobic Surfaces for Drag Reduction. *Phys. Rev. Lett.* **2011**, *106*, No. 014502.

(12) Lv, P.; Xue, Y.; Shi, Y.; Lin, H.; Duan, H. Metastable States and Wetting Transition of Submerged Superhydrophobic Structures. *Phys. Rev. Lett.* **2014**, *112*, 196101.

(13) Hof, B. Water Flows out of Touch. *Nature* **2017**, *541*, 161−162.

(14) Deng, X.; Mammen, L.; Butt, H. J.; Vollmer, D. Candle Soot as a Template for a Transparent Robust Superamphiphobic Coating. *Science* **2012**, *335*, 67−70.

(15) Zhan, Z.; Li, Z.; Li, X.; Garcell, E.; Singh, S.; ElKabbash, M.; Guo, C. Creating Superhydrophobic Polymer Surfaces with Superstrong Resistance to Harsh Cleaning and Mechanical Abrasion Fabricated by Scalable One-Step Thermal-Imprinting. *Adv. Mater. Interfaces* **2019**, *6*, 1900240.

(16) Mlot, N. J.; Tovey, C. A.; Hu, D. L. Fire Ants Self-Assemble into Waterproof Rafts to Survive Floods. *Proc. Natl. Acad. Sci. U. S. A.* **2011**, *108*, 7669−7673.

(17) Seymour, R. S.; Hetz, S. K. The Diving Bell and the Spider: the Physical Gill of Argyroneta Aquatica. *J. Exp. Biol.* **2011**, *214*, 2175−2181.

(18) Koh, J. S.; Yang, E.; Jung, G. P.; Jung, S. P.; Son, J. H.; Lee, S. I.; Jablonski, P. G.; Wood, R. J.; Kim, H. Y.; Cho, K. J. Jumping on Water: Surface Tension-Dominated Jumping of Water Striders and Robotic Insects. *Science* **2015**, *349*, 517−521.

(19) Pan, Q.; Liu, J.; Zhu, Q. A Water Strider-Like Model with Large and Stable Loading Capacity Fabricated from Superhydrophobic Copper Foils. *ACS Appl. Mater. Interfaces* **2010**, *2*, 2026−2030.

(20) Yong, J.; Zhan, Z.; Singh, S. C.; Chen, F.; Guo, C. Femtosecond Laser-Structured Underwater "Superpolymphobic" Surfaces. *Langmuir* **2019**, *35*, 9318−9322.

(21) Feng, L.; Li, S.; Li, Y.; Li, H.; Zhang, L.; Zhai, J.; Song, Y.; Liu, B.; Jiang, L.; Zhu, D. Super-Hydrophobic Surfaces: From Natural to Artificial. *Adv. Mater.* **2002**, *14*, 1857−1860.

(22) Chu, D.; Singh, S. C.; Yong, J.; Zhan, Z.; Sun, X.; Duan, J.-A.; Guo, C. Superamphiphobic Surfaces with Controllable Adhesion Fabricated by Femtosecond Laser Bessel Beam on PTFE. *Adv. Mater. Interfaces* **2019**, *6*, 1900550.

(23) Sun, T.; Wang, G.; Feng, L.; Liu, B.; Ma, Y.; Jiang, L.; Zhu, D. Reversible Switching between Superhydrophilicity and Superhydrophobicity. *Angew. Chem., Int. Ed.* **2004**, *43*, 357−360.

(24) Vorobyev, A. Y.; Guo, C. Direct femtosecond laser surface nano/microstructuring and its applications. *Laser & Photonics Review* **2013**, *7*, 385−407.

(25) Fadeeva, E.; Schlie, S.; Koch, J.; Chichkov, B. N.; Vorobyev, A. Y.; Guo, C. Femtosecond Laser-Induced Surface Structures on Platinum and Their Effects on Surface Wettability and Fibroblast Cell Proliferation. *Contact Angle, Wettability and Adhesion* **2009**, *6*, 163−172.

(26) Kietziga, A. M.; Mirvakilia, M. N.; Kamalb, S.; Englezosa, P.; Hatzikiriakosa, S. G. Nanopatterned Metallic Surfaces: Their Wettability and Impact on Ice Friction. *J. Adhes. Sci. Technol.* **2011**, *25*, 1293−1303.

(27) Vorobyev, A. Y.; Guo, C. Metal pumps liquid uphill. *Appl. Phys. Lett.* **2009**, *94*, 224102.

(28) Chu, D.; Singh, S. C.; Zhan, Z.; Sun, X.; Duan, J.-A.; Guo, C. Creation of Enhanced Transmission for Clear and Frosted Glass through Facile Surface Texturing. *Opt. Mater. Express* **2019**, *9*, 2946−2954.

(29) He, Y.; Zhang, J.; Singh, S.; Garcell, E.; Vorobyev, A. Y.; Lam, B.; Zhan, Z.; Yang, J.; Guo, C. Maskless Laser Nano-Lithography of Glass through Sequential Activation of Multi-Threshold Ablation. *Appl. Phys. Lett.* **2019**, *114*, 133107.

(30) Lu, J.; Yang, J.; Singh, S. C.; Zhan, Z.; Yu, Z.; Xin, W.; Huang, T.; Guo, C. Hierarchical Micro/nanostructured TiO_2/Ag Substrates Based on Femtosecond Laser Structuring: A Facile Route for Enhanced SERS Performance and Location Predictability. *Appl. Surf. Sci.* **2019**, *478*, 737−743.

(31) Yong, J.; Singh, S. C.; Zhan, Z.; Chen, F.; Guo, C. How To Obtain Six Different Superwettabilities on a Same Microstructured Pattern: Relationship between Various Superwettabilities in Different Solid/Liquid/Gas Systems. *Langmuir* **2019**, *35*, 921−927.

(32) Yong, J.; Singh, S. C.; Zhan, Z.; Huo, J.; Chen, F.; Guo, C. Reducing Adhesion for Dispensing Tiny Water/Oil Droplets and Gas Bubbles by Femtosecond Laser-Treated Needle Nozzles: Superhydrophobicity, Superoleophobicity, and Superaerophobicity. *ChemNanoMat* **2019**, *5*, 241−249.

(33) Feng, X.-Q.; Gao, X.; Wu, Z.; Jiang, L.; Zheng, Q.-S. Superior Water Repellency of Water Strider Legs with Hierarchical Structures: Experiments and Analysis. *Langmuir* **2007**, *23*, 4892−4896.

(34) Hu, D. L.; Chan, B.; Bush, J. W. M. The Hydrodynamics of Water Strider Locomotion. *Nature* **2003**, *424*, 663−666.

(35) Hu, D. L.; Bush, J. W. M. Meniscus-Climbing Insects. *Nature* **2005**, *437*, 733−736.

DOI: 10.1021/acsami.9b15540
ACS Appl. Mater. Interfaces 2019, 11, 48512−48517